High Power Laser Science and Engineering, (2023), Vol. 11, e58, 8 pages.
doi:10.1017/hpl.2023.40

HIGH POWER LASER SCIENCE AND ENGINEERING

RESEARCH ARTICLE

Generation of a curved plasma channel from a discharged capillary for intense laser guiding

Jian-Long Li[1], Bo-Yuan Li[2], Xin-Zhe Zhu[1], Ze-Wu Bi[1], Xin-Hui Wen[1], Lin Lu[1], Xiao-Hui Yuan[1,3], Feng Liu[1,3], and Min Chen[1,3]

[1] *Key Laboratory for Laser Plasmas (Ministry of Education), School of Physics and Astronomy, Shanghai Jiao Tong University, Shanghai, China*

[2] *Tsung-Dao Lee Institute, Shanghai Jiao Tong University, Shanghai, China*

[3] *Collaborative Innovation Center of IFSA (CICIFSA), Shanghai Jiao Tong University, Shanghai, China*

(Received 10 January 2023; revised 18 April 2023; accepted 8 May 2023)

Abstract

Straight plasma channels are widely used to guide relativistic intense laser pulses over several Rayleigh lengths for laser wakefield acceleration. Recently, a curved plasma channel with gradually varied curvature was suggested to guide a fresh intense laser pulse and merge it into a straight channel for staged wakefield acceleration [Phys. Rev. Lett. 120, 154801 (2018)]. In this work, we report the generation of such a curved plasma channel from a discharged capillary. Both longitudinal and transverse density distributions of the plasma inside the channel were diagnosed by analyzing the discharging spectroscopy. Effects of the gas-filling mode, back pressure and discharging voltage on the plasma density distribution inside the specially designed capillary are studied. Experiments show that a longitudinally uniform and transversely parabolic plasma channel with a maximum channel depth of 47.5 μm and length of 3 cm can be produced, which is temporally stable enough for laser guiding. Using such a plasma channel, a laser pulse with duration of 30 fs has been successfully guided along the channel with the propagation direction bent by 10.4°.

Keywords: curved plasma channel; discharging spectroscopy; laser guiding

1. Introduction

The natural diffraction of a laser pulse limits its focus distance within the Rayleigh length, which is a main shortcoming of laser wakefield acceleration (LWFA)[1–3]. In LWFA, strong wakefields can only be excited when the laser intensity is high enough. Several schemes to stably guide the laser pulse to distance over several Rayleigh lengths have been proposed and demonstrated in the last few decades[4–6], where a plasma channel with transversely parabolic density distribution is usually used to balance the natural diffraction[7]. In this way, electrons have been accelerated to the multi-GeV level[8]. Up to now, quasi-mono-energetic electron beams with peak energy of 7.8 GeV have been generated by guiding a relativistically intense laser pulse with a peak power of 0.85 PW over 15 Rayleigh lengths[9], which is the highest energy record in single-stage LWFA. However, due to the dephasing of the accelerated electrons, the energy depletion and the natural diffraction of the drive laser, the energy gain of an electron beam in single-stage LWFA is limited to 10 GeV based on the current laser technology and relativistic laser guiding ability, which is far from the requirement of many applications, such as TeV-level electron-positron colliders[10]. To further increase the electron energy, multi-staged LWFA by using multiple drive lasers is proposed[11]. Besides the laser guiding in a straight channel, how to guide a second relativistic laser to the straight acceleration line is another challenge for staged LWFA.

Recently, by analytical and numerical studies, Luo *et al.*[12] proposed a scheme to guide the second laser to the acceleration axis of the electrons, where a specially designed curved plasma channel was suggested. However, detailed experimental investigation of such a curved plasma channel is still lacking. In this paper, we show experimental results of curved plasma channel generation, and measurement of the plasma density distributions inside the channel.

Correspondence to: Feng Liu, Key Laboratory of Laser Plasmas (MoE), School of Physics and Astronomy, Shanghai Jiao Tong University, Shanghai 200240, China. Email: liuf001@sjtu.edu.cn

© The Author(s), 2023. Published by Cambridge University Press in association with Chinese Laser Press. This is an Open Access article, distributed under the terms of the Creative Commons Attribution licence (https://creativecommons.org/licenses/by/4.0), which permits unrestricted re-use, distribution and reproduction, provided the original article is properly cited.

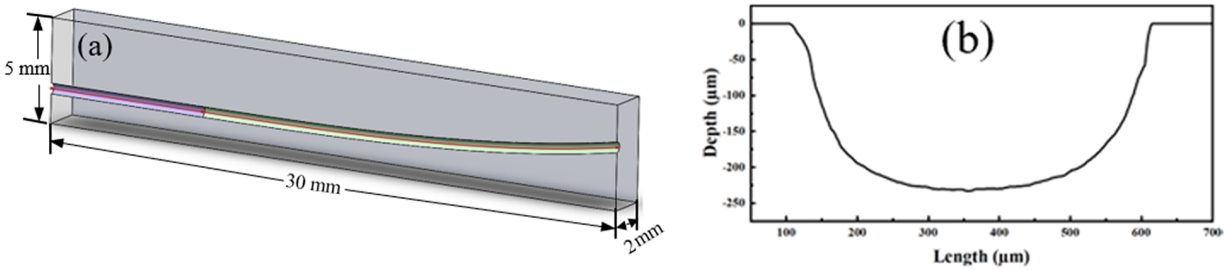

Figure 1. Design of the curved capillary: (a) schematic view of the curved plasma channel on a sapphire substrate; (b) typical cross-section of the laser etched channel on the substrate.

We tried two different gas-filling modes for the capillary and found that using two-side gas-filling ports can produce more uniform plasmas along the capillary. The dependence of transverse density distribution of the plasma channel on the back pressure and discharging voltages was also investigated.

2. Capillary fabrication and installation

Since the laser for LWFA is usually relativistic, to avoid capillary damage after a few laser shots, the requirement on the thermal and optical properties of the capillary substrate is very high. Sapphire has been proved to be an ideal material. However, it is too hard for the usual processing methods. Femtosecond laser machining is used here to fabricate our specially designed capillary. As shown in Figure 1(a), two half-curved channels were firstly etched with semicircular cross-sections on two rectangular sapphire substrates. The dimension size of the substrate is 30 mm × 2 mm × 5 mm.

The capillary is composed of two parts: a curved part with length of 22 mm and a straight part with length of 8 mm, which is geometrically tangent to the end of the curved part. The channel radius is 250 μm, as shown in Figure 1(b). According to the theoretical study, the curved part should have a varying curvature. The central line [the red line shown in Figure 1(a)] of the channel is numerically fitted by the following:

$$y = \begin{cases} 0, & 0\ \text{mm} \le x < 8\ \text{mm}, \\ \frac{(x-8)^3}{7920}, & 8\ \text{mm} \le x < 30\ \text{mm}. \end{cases} \quad (1)$$

In our experiments, two substrates are tightly clamped by a fixture to form a quasi-circular laser channel with a diameter of 500 μm.

As we know, to guide a laser pulse over several Rayleigh lengths, the refractive index of the plasma channel should balance the laser defocusing effect. A parabolic distribution of plasma density has proved to be useful for laser guiding[13–15]. A typical plasma density distribution inside the channel can be expressed as follows:

$$n(r) = n_0 + \frac{\Delta n_c r^2}{r_0^2}, \quad (2)$$

where r_0 represents the plasma channel radius and $\Delta n_c = 1.13 \times 10^{20}/r_0^2$ (μm) is the critical depth of the plasma channel. Such a plasma channel can be generated by discharging a gas-filled capillary[16,17], where the on-axis ohmic heating due to the discharging current can induce plasma expansion along the transverse direction and a parabolic plasma distribution can then be naturally formed after some time. A Gaussian laser pulse can propagate in the channel with a constant spot size when the injected laser waist equals r_0.

The discharging electric circuit and gas-filling device used in our experiments are shown in Figure 2. To control the back pressure conveniently, a gas box and two throttle valves are used. Two Parker pulse valves are employed to separate the gas flow between the gas box and the vacuum chamber. Helium gas was used in our experiments, and the gas is finally filled into the capillary by quartz or plastic pipes. An imaging grating spectrometer was used to measure the transverse plasma density distribution.

The electric circuit for high-voltage discharge is shown in the red dashed box in Figure 2. A capacitor (6 nF) is charged by the high-voltage power supply. To protect the power supply, a 5 MΩ resistor is used to limit the charging current. A neodymium-doped yttrium aluminum garnet (Nd:YAG) laser (CFR 200, Quantel Laser) and a pair of copper electrodes are combined as a trigger switch. When the laser is shot onto the copper electrodes, the trigger switch will be turned on, and the gas filled into the capillary will be ionized instantaneously. An integrated current transmitter (ICT) is used to measure the discharge current going through the capillary.

As shown in the black and violet dashed square of Figure 2, a special fixture is made to install the capillary, discharging electrodes and gas-filling ports. Two L-shaped copper discharging electrodes with holes are closely touched to the front and rear sides of the capillary. The hole diameter is a little bit larger than the inner diameter of the capillary.

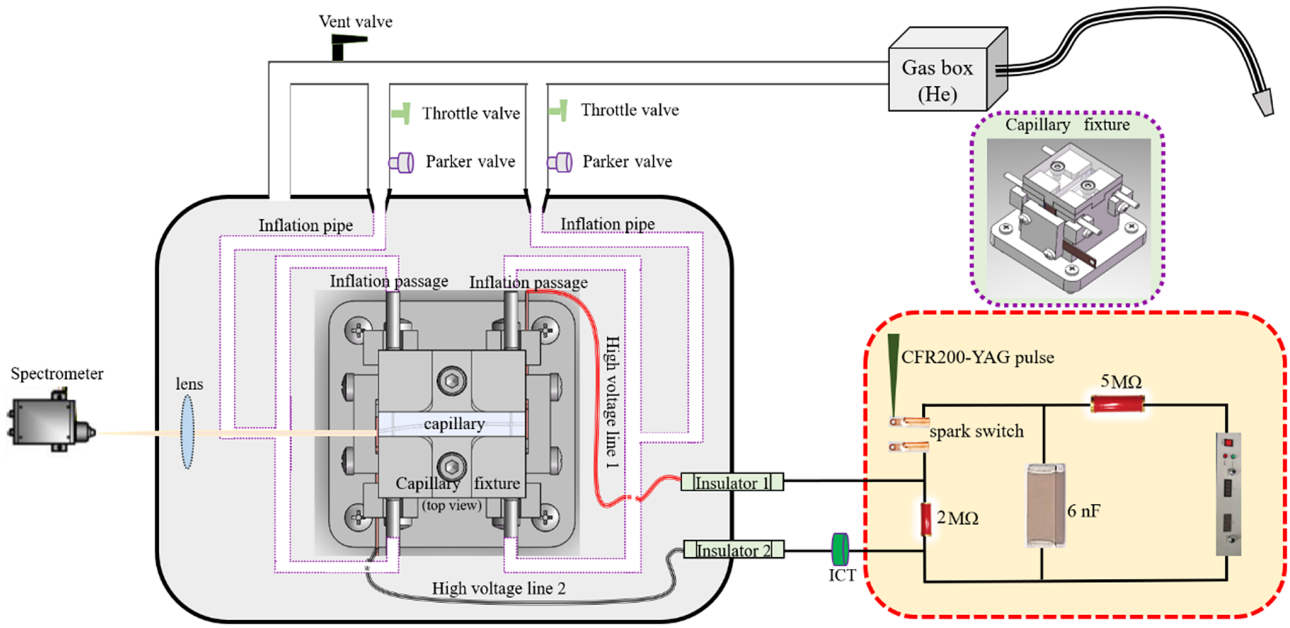

Figure 2. Schematic diagram of a plasma channel generated by high-voltage discharging of a gas-filled capillary.

Cylindrical ports are connected to the capillary along the transverse direction for filling gas. The whole clamping structure is well sealed to avoid gas leakage.

3. Diagnostic of plasma distribution inside the capillary

To get a clear picture of laser guiding, it is necessary to know both the longitudinal and transverse plasma distributions inside the capillary. When the gas is ionized by high-voltage discharge, atoms will emit characteristic lines during their transition from a high energy state to a lower one. During this process, the collisions among electrons and ions will broaden the width of the characteristic lines, which is known as Stark broadening. It can be used to calculate the plasma density. A typical relation of plasma density and the spectral width can be written as follows:

$$\lg(n_e) = a + b \times \left(\sqrt{\frac{T_e}{T_c}} + \sqrt{\frac{T_c}{T_e}} + \sqrt{\frac{T_e}{T_m \mu}} \right) + p \lg(\Delta\lambda_s), \tag{3}$$

where T_e is the plasma temperature and $\Delta\lambda_s$ is the full width at half maximum (FWHM) of the spectral line. According to Ref. [18], $a = 23.287156$, $b = 0.083064$, $p = 0.988943$, $T_c = 11{,}648$ and $T_m = 132{,}390$. We use the brightest spectral line (587.6 nm) of helium for the density calculation[19].

To diagnose the longitudinal plasma density distribution of the capillary, a light collection device with 10 optical fibers was used, as shown in Figure 3(a). The 10 fiber probes are fixed on the top surface of the capillary fixture. They are uniformly positioned along the longitudinal direction of the capillary, but the transverse position of each fiber changes with the central line of the capillary. The 10 fibers are combined to be a line and transmit the collected light to the entrance slit of the spectrometer. The spectral resolution of the spectrometer is about 0.5 nm, which is much smaller than the Stark broadening.

We first used the single-side gas-filling mode, where the gas-filling ports are on the same side of the capillary and are near the middle, as shown in Figure 4(a). The back pressure is 25 psig and the gas-filling duration is 100 ms. The discharge voltage is 20 kV. The acquisition time for the spectrometer is set to be around the first discharge current peak, as shown by the dashed box in Figure 3(b). The raw spectral image obtained by the spectrometer is shown in Figure 3(c). Since the transmission efficiency of the fibers and their coupling to the vacuum feed through on the flange are different, the spectral intensities for different fibers are not the same. However, the line width is crucial for the density calculation, rather than the brightness. The FWHM of the line can be calculated by making a Lorentz curve fitting. The plasma density is then calculated and a typical result is shown in Figure 3(d). It can be seen that under the current condition, the plasma density along the longitudinal direction is not uniform. In general, the plasma density near the center region is higher than that at the ends of the capillary.

4. Characterization of the curved plasma channel

To produce more uniform plasma density distribution along the laser propagation direction, two gas-filling modes were investigated. In the single-side gas-filling mode, the helium

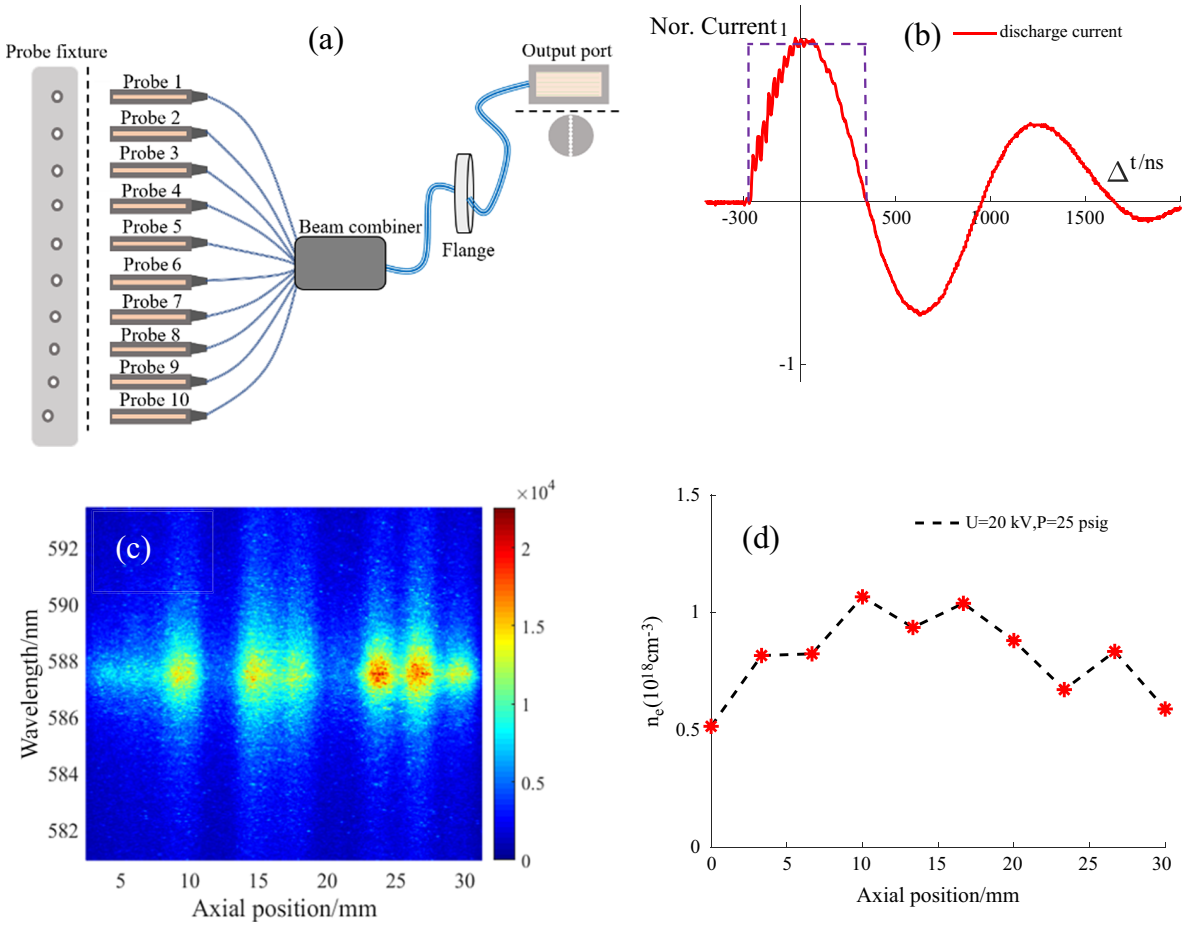

Figure 3. Scheme for plasma density measurement inside the capillary: (a) diagram of the optical fiber detector for spectrum collection; (b) normalized discharge current waveform and collection gate (labeled by the dashed box); (c) typical spectrum detected by a CCD; (d) typical calculated density distribution along the capillary.

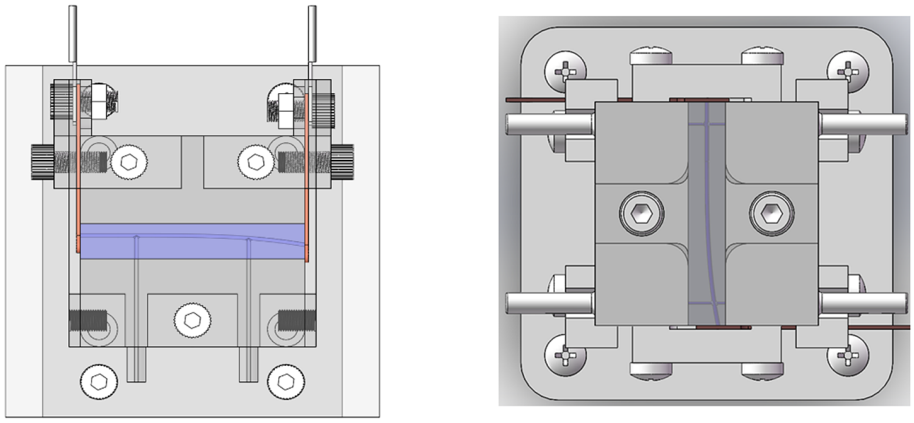

Figure 4. Effects of different gas-filling modes on the plasma density distribution: (a) single-side gas-filling; (b) two-side gas-filling.

gas is filled into the capillary from the same side of the capillary, as shown in Figure 4(a). The distances from the two gas-filling ports to their nearest capillary ends are 7.5 mm. In the two-side gas-filling mode, as shown in Figure 4(b), two pairs of gas-filling ports are fabricated on each side of the curved capillary. The distance from each port to its nearest capillary end is 3 mm.

In Figure 5 we show the plasma density distribution along the capillary with different back pressures. The gas-filling duration is set to be 100 ms by adjusting the Parker pulse

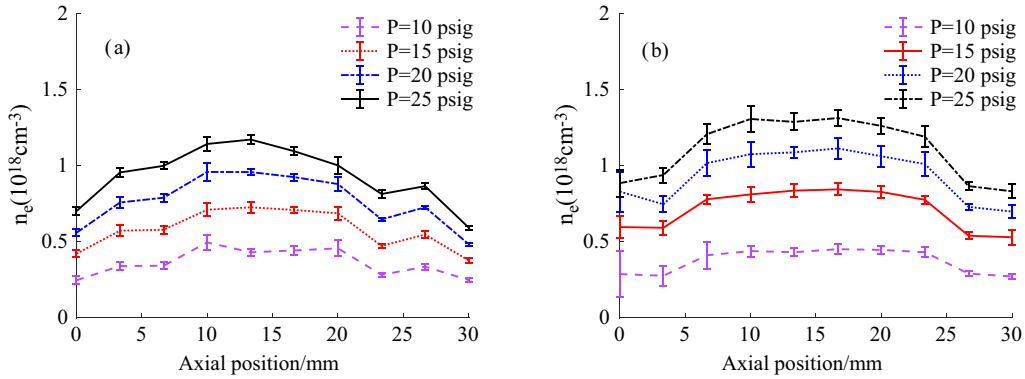

Figure 5. Plasma density distribution along the laser propagation direction in the curved capillary with different back pressures: (a) single-side gas-filling mode; (b) two-side gas-filling mode. The discharge voltage is 22 kV.

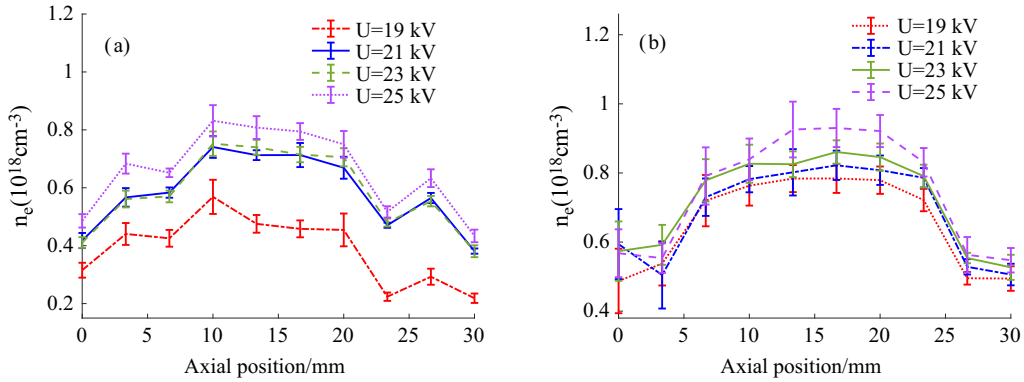

Figure 6. Effects of the discharge voltage on the longitudinal plasma density distribution: (a) single-side gas-filling mode; (b) two-side gas-filling mode. Here the back pressure is fixed to be 15 psig for all cases.

valves. The discharge voltage is 22 kV. The error bars in the figures represent the standard deviation of 10 measurements. All data are collected by a charge-coupled device (CCD) within a duration of 750 ns, as shown on the discharge waveform in Figure 3(b).

The results show that when the back pressure is 10 and 15 psig, a uniform plasma density distribution can be generated inside the capillary for both gas-filling modes. However, when the back pressure is over 20 psig, the density distribution is obviously higher around the middle of the capillary. Further, a low-density trap is always formed around the position $x \approx 23$ mm for the single-side gas-filling mode. Our Ansys simulation shows this is due to the formation of local gas vortices near the gas-filling port. However, as shown in Figure 5(b), when the two-side gas-filling mode is used, the density distribution is more uniform. There is a flat region between 6 and 24 mm inside the capillary. For both gas-filling modes, the plasma density increases with the back pressure.

We then studied the effects of discharge voltage on the longitudinal plasma density distribution. Figure 6 shows the density distributions when different gas-filling modes and discharging voltage are used. As one can see, for both cases the plasma density is higher at higher discharge voltage. For the two-side gas-filling mode, more uniform plasma density distribution can be generated within 7–23 mm inside the capillary when the discharge voltage is 19 kV. The plasma density near the middle of the capillary is significantly higher as the discharge voltage increases to 25 kV. Overall, the plasma density distribution is more uniform in the two-side gas-filling mode. In this mode, the plasma density distribution is also less sensitive to the discharge voltage.

For relativistic laser guiding, besides the longitudinal plasma distribution, a transversely parabolic plasma channel is essential. The discharging plasma at the capillary end is imaged onto the slit of an imaging grating spectrometer, so a spatially resolved spectrum of the plasma is obtained. We then use Equation (3) to calculate the plasma density for each transverse position. In this way, we get the transverse density distribution. Figures 7(a) and 7(b) show the raw spectral images when the back pressure is 15 and 30 psig, respectively. The acquisition time for the spectrometer in both cases is 250 ns and the discharge voltage is 22 kV.

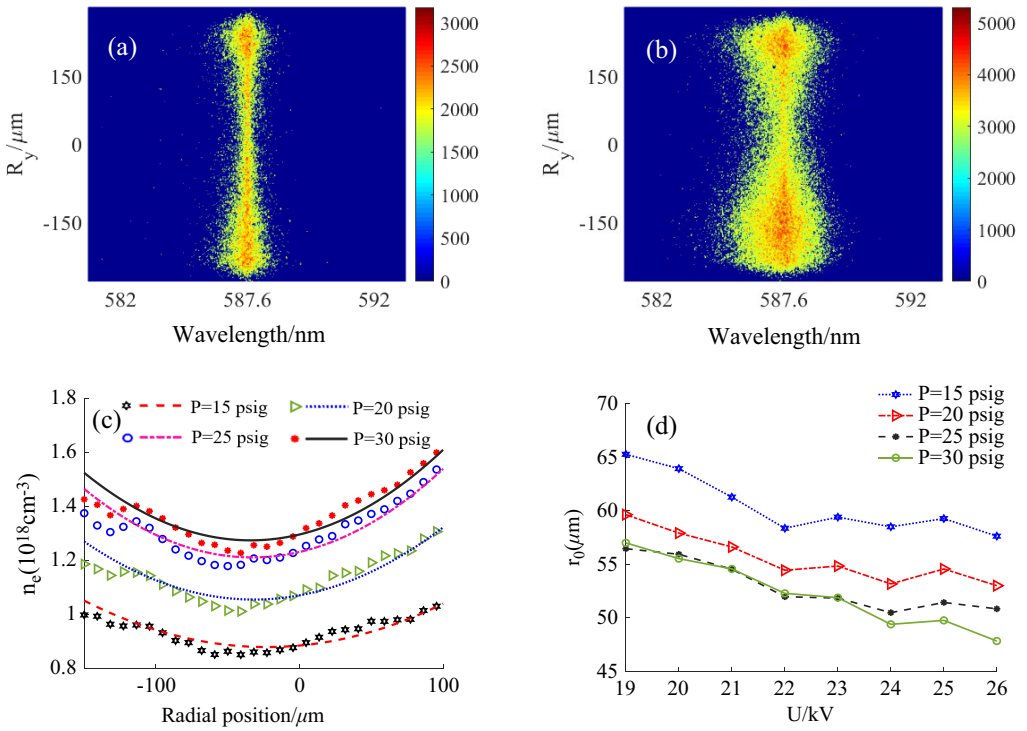

Figure 7. Measurement of the radial plasma density distribution: (a), (b) raw spectral images when the gas back pressure is 15 and 30 psig, respectively; (c) effects of back pressure on the radial plasma density distribution, where the marked results are measured and the curves are fitted; (d) dependence of the channel radius (r_0) on the discharge voltage. The discharge voltage for (a), (b) and (c) is 22 kV.

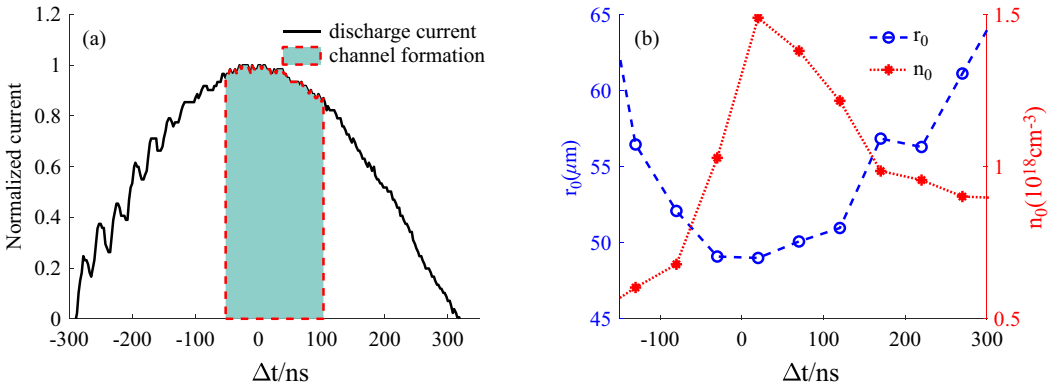

Figure 8. Temporal evolution of a plasma channel: (a) normalized discharge current in the capillary; (b) evolution of r_0 and n_0 when the back pressure is 25 psig and the discharge voltage is 26 kV.

The images show obviously narrower line widths around the channel central region, which means the density there is much lower.

Figure 7(c) shows the measured plasma density distribution along the radial direction when different back pressures are used. It can be seen that the electron density increases with gas back pressure. However, for all cases, the plasma density around the central region is obviously lower than that at the edge regions. Owing to the asymmetry of the capillary used in the experiment, the minimum values of the transverse density distributions are not at the zero points along the radial direction. However, the density distribution still shows a parabolic profile, as shown by the fitted lines. The radii of the channels (r_0) are calculated from the fitted lines. Figure 7(d) shows the variation of r_0 with different discharge voltages. It can be seen that when the discharge voltage increases from 19 to 26 kV, r_0 gradually decreases. The reason is that the higher voltage brings stronger ohmic heating. It thus enhances the thermal expansion of the plasma and results in a deeper channel (i.e., small r_0). Furthermore, when the back pressure increases, the number of electrons involved in the thermal expansion increases, which favors the formation of a deeper plasma channel.

In Figure 8(a) we show the temporal evolution of the normalized discharge current in the capillary. We set the moment of maximum discharge current to be $t = 0$.

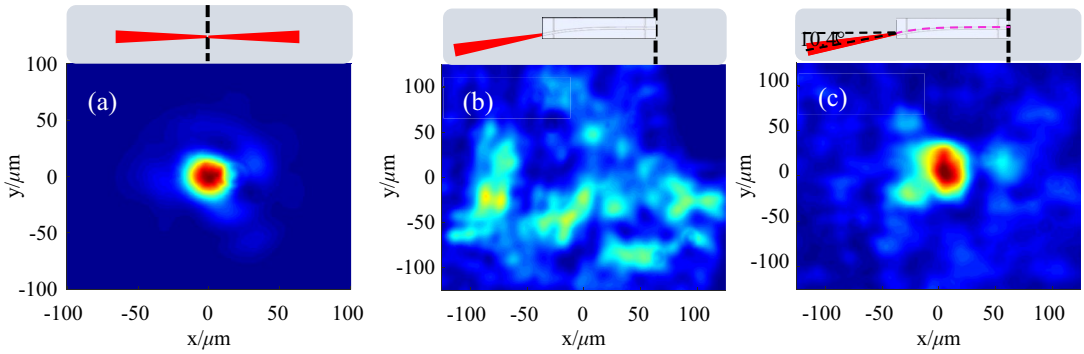

Figure 9. (a) Focused laser spot at the entrance of the curved capillary in a vacuum. (b) Laser spot at the exit of the curved capillary without discharging. (c) Guided laser spot at the exit of the curved capillary with discharging.

Experiments show that at this instant the channel radius r_0 reaches its minimum and the on-axis density n_0 reaches its maximum, as shown in Figure 8(b). When the discharge current through the capillary gradually increases, the number of ionized electrons increases as well. Simultaneously, the ohmic heating expels more electrons around the central region, which deepens the plasma channel. In contrast, when the current decreases, the thermal expansion is weakened, so the plasma channel becomes shallower. From Figure 8(b), we found that in our experiments the deepest plasma channel can be 47.5 μm, and it lasts from –20 to 50 ns. After that, the plasma channel gradually disappears. We also found that the channel radius is less than 50 μm for the period from –50 to 100 ns, corresponding to the shadowed area in Figure 8(a). Such a stable period is long enough to guide a second laser for multi-staged LWFA by using the curved plasma channel.

5. Laser guiding in the curved plasma channel

To show the guiding ability of the curved plasma channel, a laser pulse with duration of 30 fs (FWHM) and central wavelength of 800 nm was used in experiment. Due to the space limitation of our current experimental layout, the relativistic laser guiding cannot be performed and only low-intensity laser guiding is tested. The pulse energy was kept below 10 mJ during the experiment to avoid damaging the optics.

The laser is initially focused at the entrance of the capillary by an $f/20$ off-axis parabolic mirror. A typical laser spot in a vacuum is shown in Figure 9(a). The spot diameter is about 56 μm. When the curved capillary was filled with gas but without discharging, which means the plasma channel was not formed, the laser spot at the exit of the capillary was significantly diverged due to the scattering and diffraction, as shown in Figure 9(b). As a comparison, when the helium gas was filled into the capillary and discharging was triggered, a better laser spot can be observed at the exit, as shown in Figure 9(c). The experiment shows that the laser pulse can be guided in the curved capillary and bent by 10.4°. In this guiding test, about 30% of the laser energy contained in the focal spot was successfully guided to the exit of the capillary. Relativistic laser guiding experiments will be carried out in the future.

6. Conclusions

In conclusion, we have experimentally generated a plasma channel in a curved capillary with gradually varied curvature. The results show that the axial plasma density distribution is more uniform when the two-side gas-filling mode is used. In this gas-filling mode, the radial density distribution of the plasma shows a parabolic shape, and the deepest channel with a radius of 47.5 μm can be formed. The channel properties can be tuned by controlling the back pressure and discharge voltage. The temporal evolution of the channel shows that a plasma channel can be formed at 20 ns before the peak time of the discharge current, and it can last for 150 ns. A test experiment for low-intensity laser guiding shows that the curved channel can be used to guide a femtosecond laser, which shows the potential application for future staged LWFA.

Acknowledgements

This work was supported by the National Natural Science Foundation of China (Grant Nos. 11991074 and 12225505) and the Strategic Priority Research Program of the Chinese Academy of Sciences (Grant Nos. XDA25010500, XDA25050000 and XDA17040504).

References

1. T. Tajima and J. M. Dawson, Phys. Rev. Lett. **43**, 267 (1979).
2. B. Yedierler and S. Bilikmen, Rev. Sci. Instrum. **70**, 1983 (1999).
3. W. P. Leemans and E. Esarey, Phys. Today **62**, 44 (2009).
4. L. C. Steinhauer and H. G. Ahlstrom, Phys. Fluids **14**, 1109 (1971).
5. Y. Ehrlich, C. Cohen, A. Zigler, J. Krall, and P. Sprangle, Phys. Rev. Lett. **77**, 4186 (1996).

6. S. Smartsev, C. Caizergues, K. Oubrerie, J. Gautier, J. P. Goddet, A. Tafzi, and C. Thaury, Opt. Lett. **44**, 3414 (2019).
7. P. Sprangle, E. Esarey, J. Krall, and G. Joyce, Phys. Rev. Lett. **69**, 2200 (1992).
8. W. P. Leemans, A. J. Gonsalves, H.-S. Mao, K. Nakamura, C. Benedetti, C. B. Schroeder, C. S. Tóth, J. Daniels, D. E. Mittelberger, S. S. Bulanov, J.-L. Vay, C. G. R. Geddes, and E. Esarey, Phys. Rev. Lett. **113**, 245002 (2014).
9. A. J. Gonsalves, K. Nakamura, J. Daniels, C. Benedetti, C. Pieronek, T. C. H. de Raadt, S. Steinke, J. H. Bin, S. S. Bulanov, J. van Tilborg, C. G. R. Geddes, C. B. Schroeder, C. S. Tóth, E. Esarey, K. Swanson, L. Fan-Chiang, G. Bagdasarov, N. Bobrova, V. Gasilov, G. Korn, P. Sasorov, and W. P. Leemans, Phys. Rev. Lett. **122**, 084801 (2019).
10. C. B. Schroeder, E. Esarey, C. G. R. Geddes, C. Benedetti, and W. P. Leemans, Phys. Rev. ST Accel. Beams **13**, 101301 (2010).
11. S. Steinke, J. Van Tilborg, C. Benedetti, C. G. R. Geddes, C. B. Schroeder, J. Daniels, K. K. Swanson, A. J. Gonsalves, K. Nakamura, N. H. Matlis, B. H. Shaw, E. Esarey, and W. P. Leemans, Nature **530**, 190 (2016).
12. J. Luo, M. Chen, W. Y. Wu, S. M. Weng, Z. M. Sheng, C. B. Schroeder, D. A. Jaroszynski, E. Esarey, W. P. Leemans, W. B. Mori, and J. Zhang, Phys. Rev. Lett. **120**, 154801 (2018).
13. S. M. Hooker, D. J. Spence, and R. A. Smith, J. Opt. Soc. Am. B **17**, 90 (2000).
14. X. Z. Zhu, B. Y. Li, F. Liu, J. L. Li, Z. W. Bi, L. Lu, X. H. Yuan, W. C. Yan, M. Chen, L. M. Chen, Z. M. Sheng, and J. Zhang, Acta. Phys. Sin. **71**, 095202 (2022).
15. L. Yu, H. M. Zhao, Q. Cao, X. Z. Zhu, J. L. Li, B. Y. Li, F. Liu, M. Chen, and Z. M. Sheng, Plasma Phys. Control. Fusion **64**, 075009 (2022).
16. T. Hosokai, M. Kando, H. Dewa, H. Kotaki, S. Kondo, N. Hasegawa, K. Nakajima, and K. Horioka, Opt. Lett. **25**, 10 (2000).
17. E. W. Gaul, S. P. Le Blanc, A. R. Rundquist, R. Zgadzaj, H. Langhoff, and M. C. Downer, Appl. Phys. Lett. **77**, 4112 (2000).
18. A. Yu Nikiforov, C. Leys, M. A. Gonzalez, and J. L. Walsh, Plasma Sources Sci. Technol. **24**, 034001 (2015).
19. H. R. Griem, M. Baranger, A. C. Kolb, and G. Oertel, Phys. Rev. **125**, 177 (1962).